Analytical Methods

PAPER

Cite this: DOI: 10.1039/c6ay00391e

Catalyst free vapor–solid deposition of morphologically different β-Ga_2O_3 nanostructure thin films for selective CO gas sensors at low temperature

K. Girija,*[a] S. Thirumalairajan,*[b] Valmor R. Mastelaro[b] and D. Mangalaraj[a]

Received 8th February 2016
Accepted 16th March 2016

DOI: 10.1039/c6ay00391e

www.rsc.org/methods

In the present work, we have demonstrated the deposition of novel morphologically different β-Ga_2O_3 nanostructure (rod and rectangular shape) thin films prepared by a vapour solid mechanism using a temperature controllable horizontal tubular furnace without using any metal catalyst or additives. The effects of growth parameter, surface morphology and particle size on the β-Ga_2O_3 thin films were systematically investigated using electron micrograph images. X-ray diffraction patterns of the prepared films reveal preferential orientation along the (111) plane. In addition, studies of the toxic carbon monoxide (CO) gas sensing performance show that the as-prepared rod shaped β-Ga_2O_3 nanostructures show good sensitivity, short response and recovery time (49–40 s) upon exposure to CO gas at 100 °C in comparison with rectangular shape β-Ga_2O_3 (56–63 s). Through exploring the gas sensing mechanism, it is argued that the sensor performance dramatically improves due to the high surface area, particle size, shape, numerous surface active sites and the oxygen vacancies. The developed 1D β-Ga_2O_3 thin films not only possess unique shape and size, but also influence the development of various potential applications.

1. Introduction

Recent studies have demonstrated that morphology has a significant influence on the gas sensing performance of nanomaterials.[1] One-dimensional (1D) nanostructures have been extensively studied because of their specific morphology and novel properties.[2] Generally, a 1D nanostructure is constructed with a high aspect ratio, and at least one of its dimension should be below 100 nm range, no matter whether it is rod, wire, belt or tube shaped.[3] Also, 1D nanostructure materials are strong candidates for toxic gas sensing application because of their large surface-to-volume ratio, low operating temperature and the congruence of the carrier screening length with their lateral dimensions which make them highly sensitive and efficient transducers of surface chemical processes.[4–6] Synthesis and device fabrication using 1D metal oxides have attracted great attention because the properties of these oxides can be tuned by adjusting their various shapes and sizes. Controlling the shape of the nanostructure is an important step not only for scientific interests but also towards potential applications.[7–9]

Many 1D metal oxide nanomaterials such as ZnO, WO_3, SnO_2, In_2O_3 and β-Ga_2O_3 have been fabricated for detecting toxic gas due to their stable chemical transduction properties, which can reversibly convert the chemical interaction on a surface to change the electrical conductivity.[10–15] Amongst them, the stable wide-band gap monoclinic β-Ga_2O_3 possesses conduction and catalytic properties and thus has potential applications in flat-panel displays, solar energy conversion devices, batteries and low temperature gas sensor detection.[16–18] Consequently, various preparation techniques of 1D β-Ga_2O_3 nanostructures have been achieved by pulsed laser deposition, sputtering, vacuum deposition, co-precipitation, sol–gel, chemical bath deposition, hydrothermal method, *etc.*,[19–22] owing to the simplicity, the vapour deposition technique is a better method for phase purity in the preparation of thin films with a larger area. Also, it provides an easy way to dope any element in a ratio of required proportion through the deposition. This method is convenient for preparing pinhole free, homogenous, smoother thin films with the required thickness.[23]

Environmental pollution due to dangerous exhaust gases has become a serious problem with the rapid growth of the automotive industry. It is a critical problem that affects our health as it causes cancer, birth defects, and mental retardation.[24] Many toxic gases such as CO, NO, NO_2, NH_3 and O_3 are the most common and dangerous because they not only pollute the

[a]Department of Nanoscience and Technology, Bharathiar University, Coimbatore-641 046, India. E-mail: kgirija1@gmail.com; Fax: +91 422 2369106; Tel: +91 422 2369130
[b]Instituto de Física de São Carlos (IFSC), University de São Paulo, CP 369, 13560-970 São Carlos, SP, Brazil

environment but also directly affect human health. Motor vehicles, domestic stoves, gas heaters and many industries are the main source of CO production, particularly in bigger cities.[24] Commercially available gas sensors which normally operate in the range of high temperatures between 300 and 700 °C are made mainly of semiconductor based materials with higher response and recovery time (minutes).[25] There is a great demand to enhance the sensitivity of chemical sensors for various sensing applications such as monitoring and conditioning of air quality, detection of toxic gases to develop sensors which are capable of sensing gas time changes down to seconds and at low temperature.[26] Therefore a toxic gas sensor with fast response and recovery time is the need of the hour and still a great challenge. To the best of our knowledge reports on morphologically different β-Ga_2O_3 thin film-based toxic CO gas sensing sensors have not been explored in the open literature.[27]

In the present work, for the first time we have prepared different morphologies of β-Ga_2O_3 nanostructures grown on Si substrates at various temperatures. A single precursor of gallium acetylacetonate was employed as both the gallium and oxygen source for the growth of β-Ga_2O_3 nanostructures *via* a vapor–solid (VS) mechanism without using any metal catalyst or additives. The influences of growth temperature, reaction time and source to substrate distance on the morphologies were investigated. A β-Ga_2O_3 based CO gas sensor was fabricated and its sensing parameters were investigated at 100 °C.

2. Experimental procedure

2.1. Fabrication of β-Ga_2O_3 nanostructure thin films

Nanostructures of β-Ga_2O_3 were deposited on Si substrates placed inside a controllable five-zone tubular furnace *via* a catalyst free solid–vapor deposition process as shown in Fig. 1. The films deposited on Si substrates were used after being cleaned in an ultrasonic bath of acetone for 20 min, hydrofluoric acid (HF) solution for 30 s and deionised water for 10 min. The experimental set up includes a horizontal tube furnace, a rotary pump system and a gas supply system as shown in the photograph (Fig. 1a). The horizontal tube furnace consist of an inner quartz tube (inner diameter: 60 mm) and an outer ceramic tube (inner diameter: 70 mm) with a tube length of 80 cm and the vacuum maintained was 10^{-3} Torr.

Gallium acetylacetonate ($(CH_3COCHCOCH_3)_3Ga$, Aldrich, 99.99%) was used as the source material. 0.3 g of gallium source was loaded in an alumina crucible and placed at the IInd zone of the quartz tube, and the temperature was maintained at 200 °C. The cleaned Si wafers were placed at the beginning of downstream at distances of 15 and 25 cm away from the source material in the IIIrd zone. The zone III was maintained at various temperatures of 500, 700 and 900 °C, for the deposition to take place at a heating rate of 10 °C min^{-1}. The low-temperature zone was increased to 200 °C to vaporize the source after the high-temperature zone reaches the growth temperature. The system was pre-purged with carrier gas Ar for about 2–3 times and then finally evacuated by using a mechanical rotary pump. A mixture of argon (95%) and oxygen (5%) was introduced through the inlet of the furnace at the start of the reaction process. The deposition time was kept at 5, 15, 30 and 45 min. After the completion of the reaction time, Ar gas flow was stopped and the furnace was turned off. The sample was cooled down to room temperature naturally. A white layer of β-Ga_2O_3 was deposited on the surface of Si substrates.

2.2. Film characterization and property measurements

The optimized as-prepared samples obtained at various stages of preparation were subjected to systematic characterization using different techniques to understand the growth mechanism of nanostructures. The surface morphology, chemical composition, and structure of the prepared nanostructures were characterized using scanning electron microscopy (SEM-JEOL JSM-6380LV), atomic force microscopy (AFM, veeco dicaliber high value scanning probe microscope) and X-ray diffraction (XRD, Bruker Germany D8 Advance) with $CuK_{\alpha 1}$ radiation ($\lambda = 1.54$ Å). The Raman spectrum of the prepared samples was obtained using a LabRAM HR 800 micro Raman with a 514 nm Ar ion laser (10 mW). X-ray photoelectron spectroscopy (XPS) measurements were carried out on a ESCA + Omicron UK XPS system with a MgK_{α} source at a photon energy of 1486.6 eV. All the binding energies were referenced to the C 1s peak at 284.6 eV of the surface adventitious carbon. The thickness of the deposited film was measured by using a Tencor Alpha-step profiler.

2.3. Gas sensor system and property measurements

A home built testing chamber was used for sensing the characteristics of the β-Ga_2O_3 thin films. The ceramic tube containing the sample was placed inside the furnace maintained at the required temperature controlled with a PID temperature controller. Electrical measurements were carried out in the range from 100 to 250 °C, under a dry synthetic air or CO total stream of 50 sccm, and the sensor resistance data were collected in the four point mode. CO coming from certified bottles can be further diluted at a given concentration by mass flow controllers. The concentration of target gas was varied from 1 to 5 ppm. The sensor test devices were equilibrated in dry air at each temperature before the beginning of sensor measurement to ensure stable and reproducible baseline resistance. The change in oxide ion pumping current was measured by the dc two-probe method. In the amperometric mode, dc 1 V was applied using a potentiostat/galvanostat (Hokuto Denko, HA301) as the active electrode and a positive one. The current was measured with a digital electrometer (Advantest, model R8240). The n-type β-Ga_2O_3 was used to sense the reducing gas CO whose response is defined as $S = R_{air}/R_{gas}$, where S is the ratio of the resistance in air (R_{air}) and the sensor resistance was measured when exposed to the target reducing gas (R_{gas}). The changes in electrical resistance of the film during the process of injection and venting of CO vapor were monitored using a LabVIEW controlled data acquisition system. During the measurements, the humidity was under controlled conditions within the range of 50–55% RH.

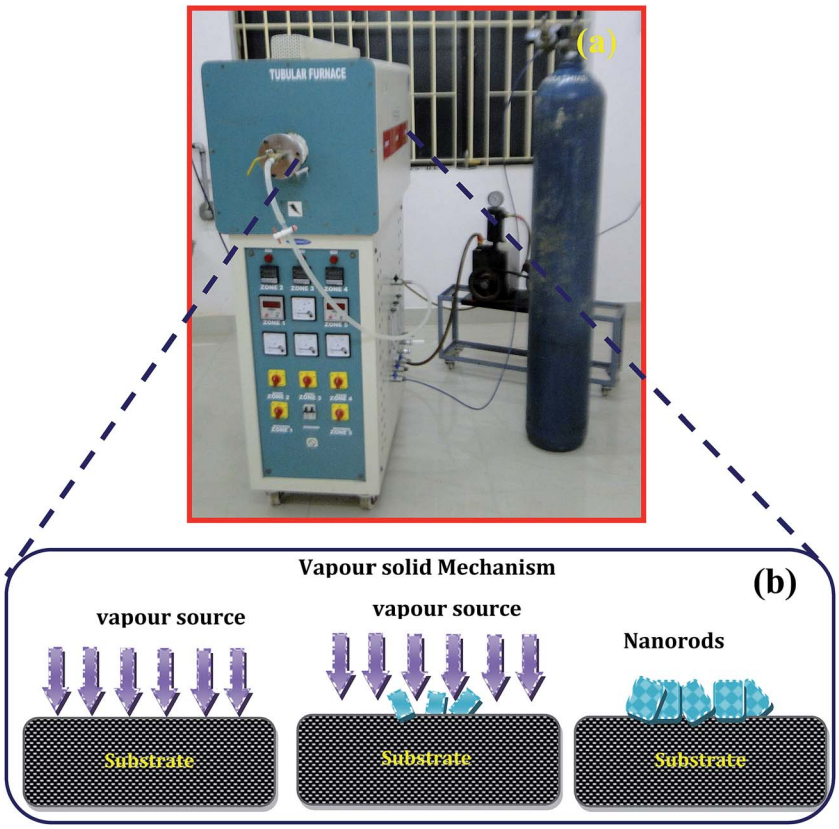

Fig. 1 (a) Photograph of the tubular furnace unit, (b) schematic illustration of the vapor–solid (VS) mechanism.

3. Results and discussion

3.1. Morphology analysis of β-Ga_2O_3 nanostructured thin films

3.1.1. Effect of deposition time and source to substrate distance on the formation of β-Ga_2O_3 nanostructured thin films. The effect of deposition time on the formation of nanostructured β-Ga_2O_3 thin films was studied at various deposition times of 5, 15, 30 and 45 min. From Fig. 2a it was observed that at 5 min of deposition time, the surface of the film was rough with the formation of agglomerated particles dispersed uniformly throughout the surface. This indicates the onset of nucleation at this particular deposition time.

Further with the increase in the deposition time to 15 min, nanorod-like structures were obtained as shown in Fig. 2b. The nanorods of β-Ga_2O_3 grown on the surface of the Si substrate were found to be uniform along their length and width. The average diameter of the nanorods was ~60 nm with a length of

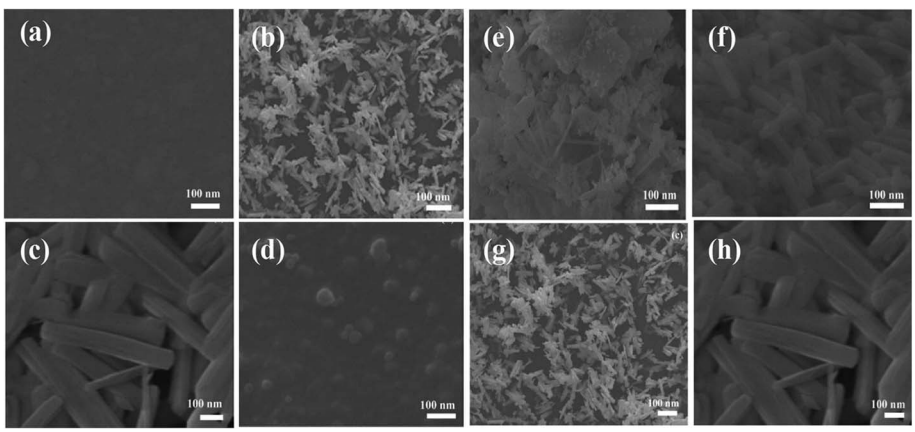

Fig. 2 Nanostructured thin films of β-Ga_2O_3 at different reaction times (a) 5 min, (b) 15 min, (c) 30 min, and (d) 45 min, at source to substrate distances of (e) 15 cm, (f) 20 cm, (g) 25 cm and (h) 30 cm.

~150 nm. Densely and closely packed nanorods were grown at a deposition time of 30 min. These nanorods are different from those prepared at 15 min. As the deposition time increased, the nanorods grow along their length and width. These rectangular shapes were found to have an average diameter of about 90 nm and a length of about 800 nm as observed in Fig. 2c. However, on further increasing the deposition time to 45 min, it was surprising to note that no interesting morphology was grown on the substrate as shown in Fig. 2d, only circular structures were observed on the surface of the film. The source to substrate distance was fixed at 25 cm while varying the deposition time. The morphology results indicate that the deposition time has influenced the growth of nanostructures formed on the surface of Si substrates. This clearly points out that the deposition time is one of the important parameters involved in determining the growth of nanostructured β-Ga_2O_3 thin films.

In addition, to estimate the effect of source to substrate distance on the formation of one dimensional nanostructure β-Ga_2O_3 thin films, deposition was carried out at distances of 15, 20, 25 and 30 cm between the source and substrate. It is worthy to mention that, in the present work the gallium source was placed in zone II of the tubular furnace, maintained at a lower temperature of 500 °C. The Si substrates used for deposition were placed in zone III, where a higher temperature of 900 °C was maintained for the films to be deposited. The nanorods were not fully formed when the distance was fixed at 15 cm and the temperature was maintained at 900 °C (Fig. 2e). Though nanorod like structures were formed at a distance of 20 cm, they are not uniform and well dispersed. Few assembled structures were also observed as noticed in Fig. 2f. Nanorods of β-Ga_2O_3 with a uniform length and diameter were obtained at a source to substrate distance of 25 cm having a thickness of 60 nm (Fig. 2g). While increasing the distance to 30 cm and at a deposition time of 30 min, closely packed rectangular nanorods with a thickness of 90 nm were obtained as in Fig. 2h. From these results it can be concluded that the source to substrate distance along with reaction time and deposition temperature play a vital role in the formation of these β-Ga_2O_3 nanostructured thin films with morphologies of nanorods having reduced size and rectangular nanorods with a larger diameter and length.

3.1.2. Effect of substrate temperature on the formation of β-Ga_2O_3 thin films. To systematically study the correlation between the substrate temperature and the growth of nanostructures, β-Ga_2O_3 nanostructured thin films were deposited at various temperatures of 500, 700 and 900 °C. The morphological results were analysed using SEM images presented in Fig. 3. Agglomerated particles were observed on the surface of the thin films deposited at a temperature of 500 °C.

There is no significant distinction between the films deposited for 15 and 30 min at 500 °C as shown in Fig. 3a and b. Since no interesting nanostructures were formed at 500 °C of substrate temperature, further the temperature was increased to 700 °C. Fig. 3c and d reveal the rod like structures deposited at 700 °C for 15 and 30 min of duration. This indicates that the formation of β-Ga_2O_3 nanostructures occurs at a higher temperature. The film deposited at a lower duration of 15 min shows that the nanorods grown on the substrate are dispersed as noticed in Fig. 3c. In contrast, for 30 min of deposition time, high yields of nanorods were obtained and they are closely placed to each other on the surface of the Si substrate as observed in Fig. 3d. Further, to understand the mechanism of the growth process of these nanostructured thin films of β-Ga_2O_3, the films were deposited at 900 °C for 15 and 30 min. The film representing 15 min of deposition time (Fig. 3e) showed no significant change in its morphology, while the film at a higher deposition time revealed the changes in the average size of nanostructures. The growth of nanorods was enormous and the average diameter was found to be 90 nm, while the length of these nanostructures were two to three times greater than the nanorods obtained at 15 min of deposition time. The rectangular nanorods were found to have smooth surfaces. These morphological results obtained by the systematic investigation of the films prepared at different deposition temperatures of 500, 700 and 900 °C indicate the enhancement of the growth rate of the rod-like structures as the temperature increases.

In the present work, no metal catalyst was used and no particles were found on the top of the nanostructures. Therefore, the growth mechanism of the nanomaterials can be understood on the basis of a self-catalytic vapor–solid (VS) mechanism. We suggest three basic steps that could have taken place during the growth of oxide nanorods: (1) diffusion of

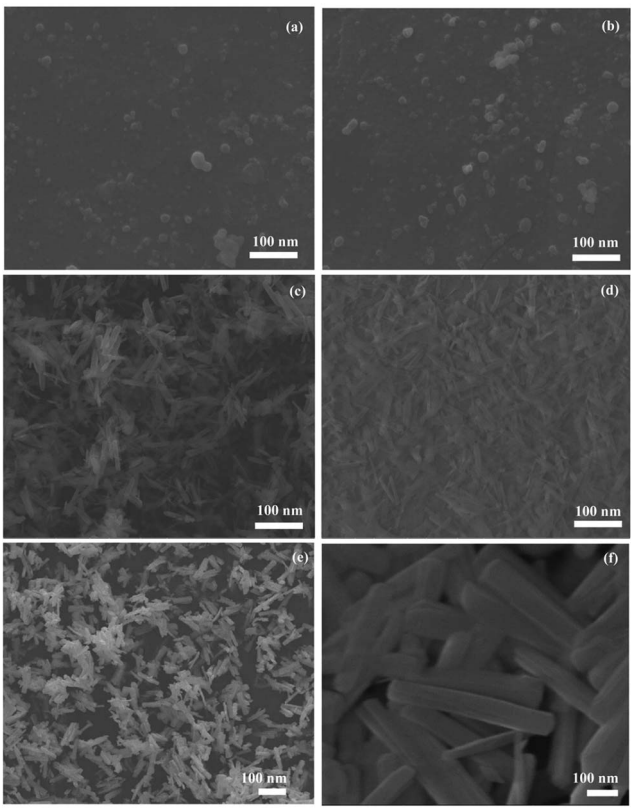

Fig. 3 Nanostructured thin films of β-Ga_2O_3 (a and b) 500 °C for 15 and 30 min, (c and d) 700 °C for 15 and 30 min and (e and f) 900 °C for 15 and 30 min.

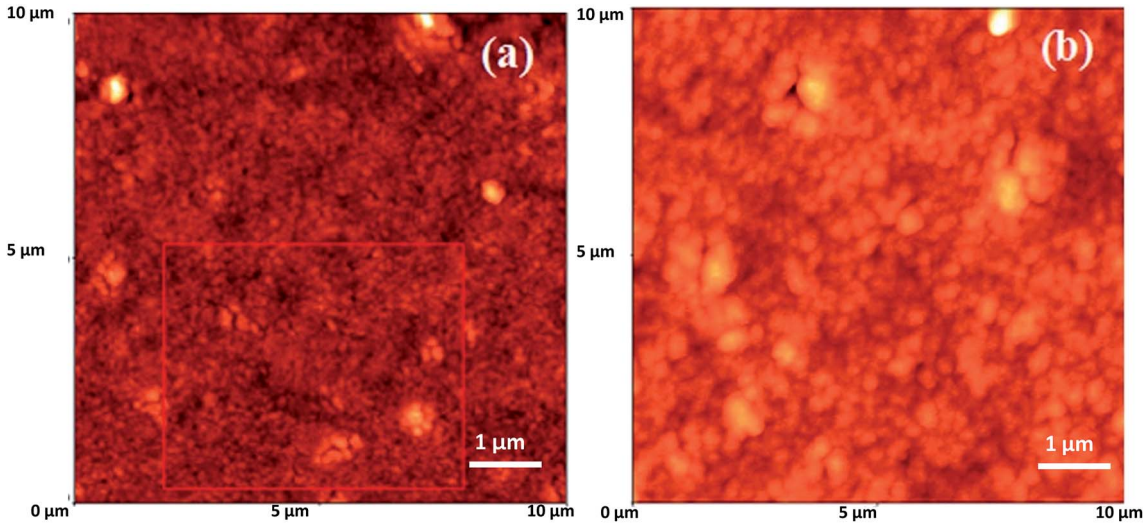

Fig. 4 AFM images of β-Ga_2O_3 thin films (a) nanorods and (b) rectangular nanorods.

oxygenated gallium, (2) nucleation on the substrate and (3) homoepitaxial growth of nuclei. The evaporation of gallium is initiated when the temperature reaches 200 °C, and then the gallium vapor reacts with O_2 which may be originated from residual oxygen in the chamber also from the carrier gas containing 5% of O_2 to become Ga_2O vapor (eqn (1)).

$$Ga + O_2 \rightarrow Ga_2O\rightarrow \quad (1)$$

$$Ga_2O + O_2 \rightarrow Ga_2O_3\rightarrow \quad (2)$$

When the partial pressure of Ga_2O in the vapor phase is high enough, the Ga_2O will deposit on the Si substrate resulting in nucleation of nanostructure gallium oxide nuclei. And then, the Ga_2O is further oxidised to Ga_2O_3 (eqn (2)). The difference in morphology of nanomaterials is considered to originate from different nuclei under different zone temperatures or other reaction parameters. Although the difference among the parameters is small, it is high enough to affect the growth process. Because both the size of nucleus and the Ga_2O vapor partial pressure are determined by the parameters discussed above. The surface dynamics of nuclei on initial nucleation of gallium oxide determines if the resulting nanostructure would be a nanowire, nanotube, nanorod or any other morphology.[26] By analysing the effect of various parameters on the thin film deposition, the films prepared at 15 and 30 min of deposition time at 900 °C at a source to substrate distance of 25 and 30 cm having the morphology of nanorods and rectangular shape nanorods are considered as optimized samples. The nanorods with a reduced diameter and the other with a longer length named rectangular nanorods are chosen and subjected to further characterization in the present work.

3.2. Topographical analysis

The surface topography of the prepared nanostructured β-Ga_2O_3 thin films was obtained at five different locations, and the average RMS roughness and grain size values were determined. Fig. 4a shows the 2D representation, from which it is inferred that the nanorod structures have a random arrangement along the surface of the substrate. The nanostructures are formed with highly interconnected particles. The average depth

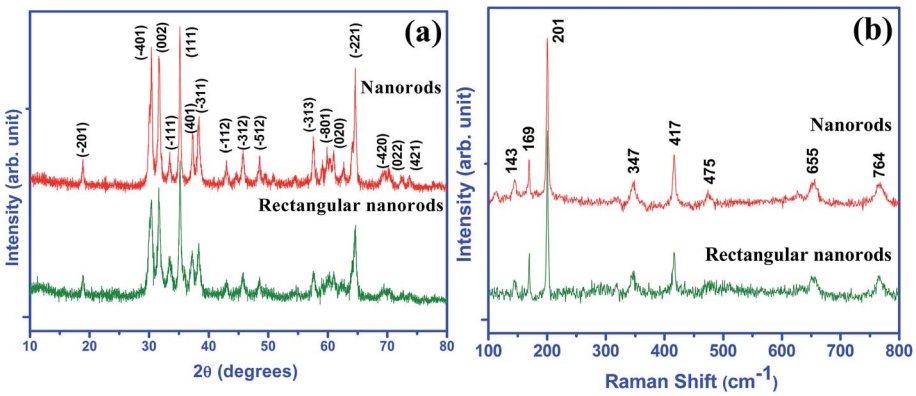

Fig. 5 (a) XRD pattern (b) Raman spectrum of morphologically different β-Ga_2O_3 nanostructured thin films.

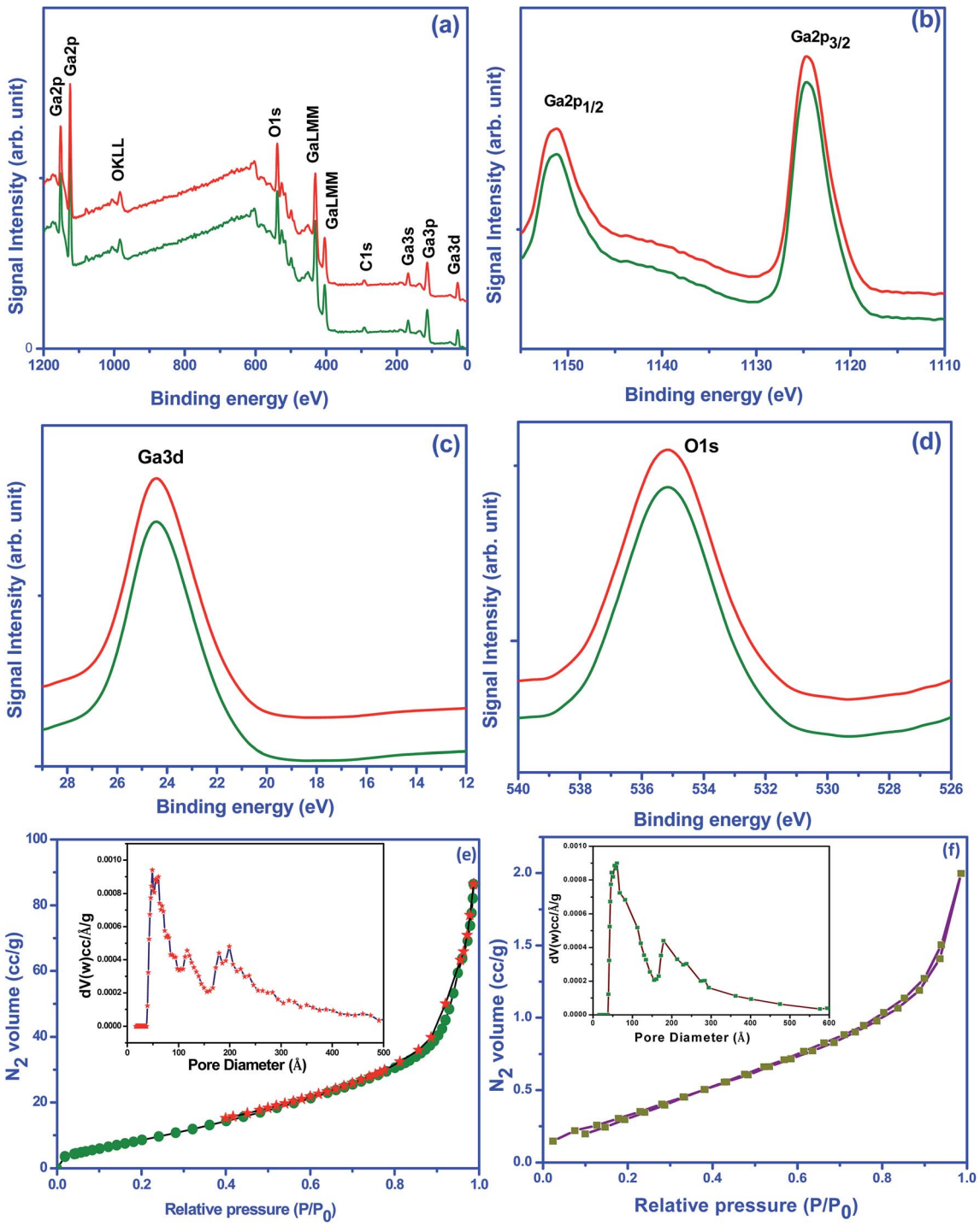

Fig. 6 (a) XPS survey spectrum of rectangular (red colour) and rod (green colour) shaped nanostructures, (b) Ga 2p, (c) Ga 3d, (d) O 1s of morphologically different β-Ga_2O_3 thin films, (e) and (f) nitrogen adsorption–desorption isotherm of the rectangular and rod (inset) shaped nanostructures the corresponding pore size distribution.

of each pore-like appearance held between rod structures is ~56.06 nm with a RMS roughness of 6.13 nm, and the well-defined grain boundaries are also observed within the scanning area.

Further the films are composed of nanoparticles and the film surface is condensed, uniform and smooth. Fig. 4b shows the relevant variations in the surface topography recorded for the rectangular β-Ga_2O_3 nanostructures. The topography shows the formation of longer grains. Dense growth of the structure can be noticed all over the surface. This image coincides well with the SEM images obtained for this structure, discussed in the Morphology analysis. The overall growth appears more homogeneous which shows the formation of a rectangular structure with a grain size of ~88.20 nm and a RMS roughness value of

~8.85 nm. A more uniform surface topography with grains equally distributed throughout the surface of the films can be observed. The well-defined grain boundaries are also observed when the scanning area was restricted to 2 μm. The overall thickness appears to be more homogeneous in the nanorods of β-Ga_2O_3 thin films compared to the rectangular shape. Further, single phase β-Ga_2O_3 nanostructured thin films with good crystalline quality and a clear morphology as observed in Fig. 4a and b were used for gas-sensing measurements in the present study, whose thickness was found to be ~700 and ~800 nm, respectively.

3.3. Structural analysis

The phase structure and crystallinity of β-Ga_2O_3 rods and the rectangular rods grown at a temperature of 900 °C with the source to substrate distance maintained at 25 and 30 cm were analysed from the XRD patterns of the respective nanostructured thin films shown in Fig. 5a. For both the nanostructured samples, the diffraction peaks exhibit a strong and sharp intensity, which indicates the increased crystallinity of the sample. The lattice constants derived from the peak positions were approximately the same for both the samples, a = 12.227, b = 3.038, c = 5.807 Å, $\alpha = 90°$, $\beta = 103.7°$ and $\gamma = 90°$ with a maximum experimental error of ±0.002, which is in accordance with the monoclinic β-Ga_2O_3 phase with space group $C2/m$ as reported in JCPDS 41-1103.[28] The diffraction peak (111) shows high intensity for both the rods and rectangular nanostructures. No other phases were observed in both the samples within the detection limit for β-Ga_2O_3 nanostructured thin films, thus confirming the phase purity of the prepared samples. The average crystallite size calculated using the Debye–Scherrer formula[29] was found to be ~87 nm for rectangular nanostructures and ~59 nm for nanorods, almost in agreement with the results obtained from the morphological analysis.

In addition, the room temperature Raman scattering spectrum of nanostructured β-Ga_2O_3 thin films having rod and rectangular rod-like morphology is shown in Fig. 5b. The Raman bands observed at 655 and 764 cm^{-1} can be attributed to ν1 symmetric stretching bands of GaO_4 tetrahedra. The bands observed in the mid frequency range can be assigned to the symmetric stretching mode of GaO_6 octahedra. The bands in the low frequency range can be attributed to O–Ga–O bending modes of the GaO_6 octahedra. The peak positions are in good agreement with the values reported for β-Ga_2O_3.[30] These results confirm that the prepared nanostructures have a single phase and the peaks corresponding to other phases were not detected, indicating high purity of the prepared thinfilms. The Raman results also agree with the results discussed in the XRD section.

3.4. Compositional analysis

The compositional analysis of β-Ga_2O_3 nanostructured thin films was carried out using X-ray photoelectron spectroscopy (XPS), a specific spectrometry for chemical bonding state analysis of the prepared materials. Fig. 6 shows the XPS spectrum of β-Ga_2O_3 nanostructured thin films for rods and rectangular shaped rods. No significant changes in the peak positions were noticed for both samples. The binding energies obtained from the XPS spectrum were corrected with the C 1s reference line at 284.6 eV. The typical XPS survey spectrum (Fig. 6a) with energy ranging from 0–1000 eV reveals the peaks of the core level from Ga 3d, Ga 2p, and O 1s states, respectively. The energy peaks positioned in the range of 1150 to 1123 eV, respectively, as in Fig. 6b, are known to stem from Ga $2p_{1/2}$ and Ga $2p_{3/2}$, representing the Ga–O bonding.[31] The energy peak of Ga 3d centred at around 24.50 eV can be ascribed to the presence of gallium in β-Ga_2O_3 (Fig. 6c). The O 1s XPS signal observed at a binding energy of 535.50 eV (Fig. 6d) corresponds to the characteristic peak of β-Ga_2O_3.[32]

The XPS analysis indicates that the material synthesized was β-Ga_2O_3 which corresponds with the XRD measurement. The

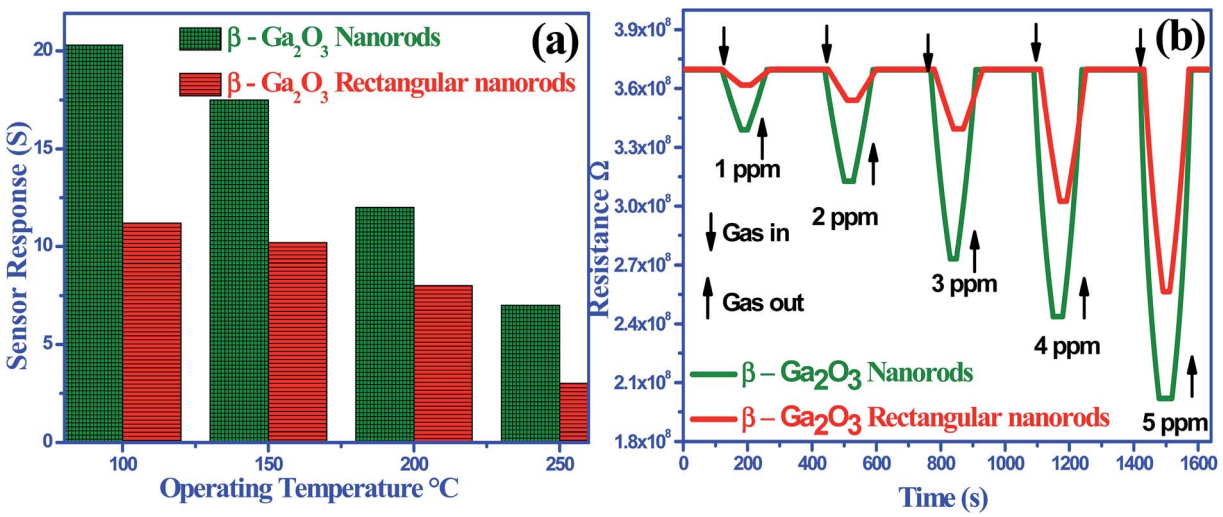

Fig. 7 (a) The response to 1 ppm of CO gas by the morphologically different β-Ga_2O_3 thin films working at different temperatures, (b) transient sensing response of β-Ga_2O_3 nanostructure thin films for different concentrations of CO at 100 °C.

quantification of peaks reveals that the atomic ratio of Ga/O equals the stoichiometric ratio of 2 : 3. The binding energy values are in agreement with the reported values.[33] This confirms that in both samples the impurity phases of organic compounds are eliminated due to high temperature deposition. Also, a kind of metal-gas molecular support interaction has been taken as an important factor in the gas-sensing mechanism.

In addition, the surface area of the optimized β-Ga_2O_3 nanostructure thinfilms was determined from the N_2 adsorption–desorption analysis as shown in Fig. 6e and f. The surface properties of nanostructures are essential to analyze, as they strongly influence the gas sensing properties of the material. Enhanced surface properties can improve the potential of nanostructures.[34] The specific surface area based on surface contact reactions for rod and rectangular nanostructures exhibits a surface area of 78 and 62 $m^2\ g^{-1}$, with a pore volume distribution of 0.12 and 0.098 $cm^3\ g^{-1}$, respectively, determined using the BJH method. Interestingly, nanorods of β-Ga_2O_3 showed a higher surface area with pore volume which can be attributed to its high porous nature and is relatively higher when compared to rectangular β-Ga_2O_3 structures. The surface area of nanostructures increases along with a decrease in their size. Therefore, the methodologies used in the present work not only opened the door to prepare precisely a controlled surface structure, but also to fabricate a high surface area and porous surface structured β-Ga_2O_3.

3.5. Gas sensing analysis of morphology dependent β-Ga_2O_3 nanostructure thin films

With a large accessible surface area, small particle size, uniform morphology and special porous structure, such novel 1D β-Ga_2O_3 nanostructures may be advantageous for toxic gas sensor applications. The fabricated sensor of β-Ga_2O_3 with different morphologies was exposed to CO gas at various temperatures between 100 and 250 °C at intervals of 50 °C as shown in Fig. 7a, to determine the optimum operating temperature of the sensor towards 1 ppm of CO. The two different morphology dependent sensors show optimal operating temperatures at which the maximum response values are achieved at 100 °C. The response value decreased correspondingly as the working temperature increased, and the maximum sensing value was 20.30 for β-Ga_2O_3 rod structures and 12.74 for the rectangular structures. The alteration of the sensor response with operating temperature is related to the adsorption and reaction that occur on the sensor surface. At the first stage, the increase in sensor response with the operating temperature is due to chemical adsorption and the reaction of gas molecules needs activation energies that must be overcome. When the

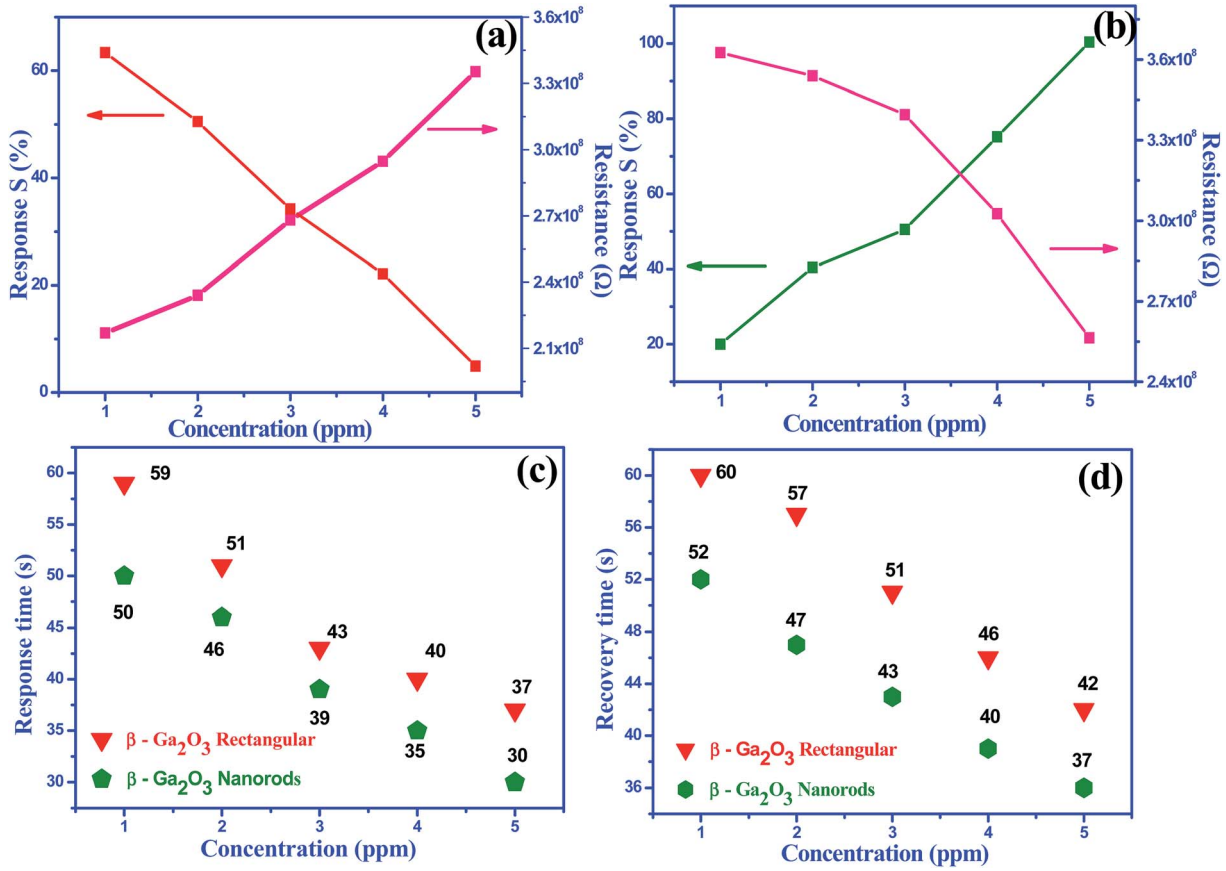

Fig. 8 Sensing response and electrical resistance as a function of CO concentration at 100 °C (a) β-Ga_2O_3 rectangular nanorods (b) β-Ga_2O_3 nanorods, (c) response time (s) and (d) recovery time (s) of different β-Ga_2O_3 nanostructure thin films.

temperature reaches the optimum operating temperature, the maximum amount of gas adsorption is reached and the reduction of CO is accelerated, resulting in the highest response. Upon further increase in the temperature, gas desorption would increase significantly leading to a decrease in the response. Therefore, we choose 100 °C as our working temperature to proceed with further analysis.

Fig. 7b shows the corresponding transient characteristics of rod and rectangular β-Ga_2O_3 nanostructure based sensors upon exposure to different CO concentrations at 100 °C with the gas flow ranging from 1 to 5 ppm. The resistance of the n-type oxide semiconductor β-Ga_2O_3 is identified to decrease upon exposure to reduction gas CO. The sensor exhibits a high response for ppm-level CO gas and the response of the sensor increases with increasing gas concentration. At the start of the gas sensing behavior, the film exposed to the synthetic dry air atmosphere exhibited higher resistance due to the oxidation reaction between the surface of the film and oxygen molecules. The test gas was then introduced into the testing chamber. When reduction gas CO is adsorbed onto the n-type β-Ga_2O_3 surface, an electron depletion layer is formed in response, resulting in the decrease of sensor resistance followed by complete recovery of its initial value when clean air was fed into the chamber. In n-type semiconducting oxides, adsorbed oxygen behaves as a surface acceptor state, accepts electrons from the valence band and hence increasing the electron concentration. In the case of rod shaped β-Ga_2O_3 samples, the response was noticeably higher with respect to the rectangular β-Ga_2O_3 nanostructure at all temperatures, which can be associated with their particle size, morphology, surface area, and particle to particle interaction.[7,8]

Fig. 8a shows the sensing response of rectangular β-Ga_2O_3 nanostructures exposed to the reduction gas CO at various concentrations of 1–5 ppm. A gradual increase in the concentration was noticed on increasing the sensor response. The sensor response was found in the range of 10.30–60.73 for 1–5 ppm of CO concentration for rectangular β-Ga_2O_3. Fig. 8b shows the response of the sensing element with a β-Ga_2O_3 nanorod morphology on exposure to CO gas, and the sensitivity was found to increase with the increase in gas concentration. The sensitivity values were determined to be in the range of 20.30–102.87. The analysis of sensing performance within an experimental error of ±0.01% demonstrates that the β-Ga_2O_3 nanorod thin films show excellent catalytic activity upon exposure to the reduction gas CO.

The response and recovery time is one of the vital parameters for toxic gas sensor applications. The response and recovery time is defined as the time taken by the sensor to achieve 90% of the total resistance variation in the case of adsorption and desorption, respectively, and the recovery time as the time necessary for the sensor to return to 10% above the original resistance in air change releasing the test gas as shown in Fig. 8c and d. It is clear that the response curves (Fig. 8b) of the sensor increases sharply with increasing concentration of CO and then returns to the baseline quickly with the CO gas exhausted out in the closed testing chamber, indicating their quick and reversible response and recovery time. Moreover, it can be seen (Fig. 8c) that the response time of the CO sensors decreases with increasing CO gas concentration. The response time decreases from 59 s to 37 s for rectangular β-Ga_2O_3 and 50 s to 30 s for β-Ga_2O_3 rod shape for 1–5 ppm CO concentration, while the recovery time (Fig. 8d) also decreases from 60 s to 42 s for rectangular β-Ga_2O_3 and 52 s to 37 s for β-Ga_2O_3 nanorod shape as the concentration increases from 1 ppm to 5 ppm. However, the observed fast response is due to the smaller grain size and uniform morphology of β-Ga_2O_3 rod structures. In β-Ga_2O_3 nanostructures, at a low concentration of 1 ppm, more CO molecules easily interact with adsorbed oxygen ions providing a fast response compared to a higher concentration.

Selectivity is another important aspect of the toxic gas sensing performance. In fact, a sensor with good selectivity can

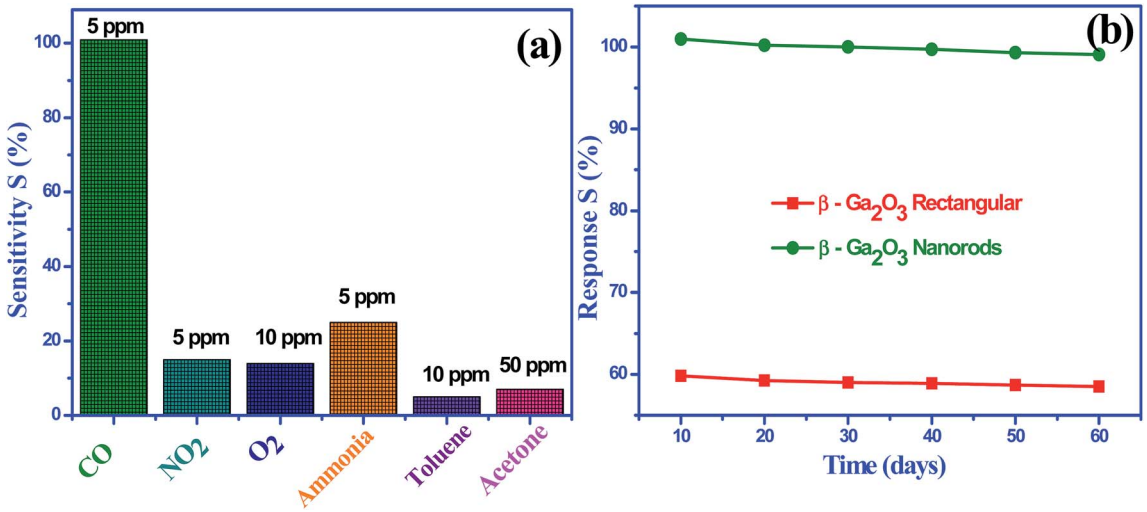

Fig. 9 (a) Sensing response of the β-Ga_2O_3 thin films towards 5 ppm of CO and other gases (b) stability of different β-Ga_2O_3 nanostructure thin film sensors at RT.

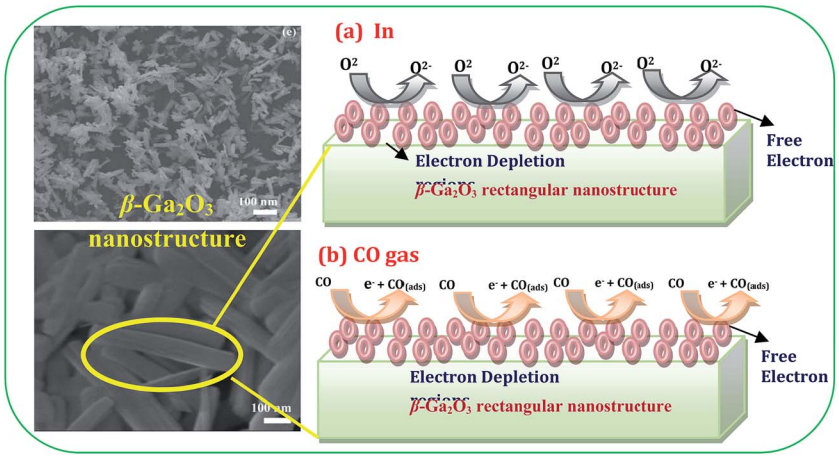

Fig. 10 Schematic diagrams for the change in sensor resistance upon exposure to air and reduction gas (CO) in the case of n-type β-Ga_2O_3 nanostructure sensing films.

be used to detect a specific target gas when it is exposed to a multi-component gas environment.[35–37] To value the selectivity of the β-Ga_2O_3 nanostructure thin film based toxic CO sensor, the fabricated sensor was exposed to six typical gases (CO (5 ppm), NO_2 (5 ppm), O_2 (10 ppm), ammonia (5 ppm), toluene (10 ppm) and acetone (50 ppm)) and the results are shown in Fig. 9a. It is noted that the β-Ga_2O_3 nanostructure thin films show a much higher response to CO than other five tested gases at low concentration, which is mainly attributed to the enhanced reaction between the acetone and the absorbed oxygen at the optimum low operating temperature, porosity of the film, particle size, and catalytic activity of β-Ga_2O_3 with CO molecules. Moreover, the electron acceptor ability of CO is higher than that of other vapors because of the presence of a lone pair of electrons.[38,39] The fabricated β-Ga_2O_3 based gas sensor is practically insensitive to the other common interference gases, showing more selectivity towards CO gas.

Furthermore, stability is another important factor of real time monitoring toxic gas sensing applications. The long-term stability of the β-Ga_2O_3 nanostructures with rectangular and rod shaped thin films was observed in response to 5 ppm of CO gas concentration, along with the baseline resistance and also the sensing response was recorded every ten days over a period of 60 days. These results are shown in Fig. 9b, which indicate that there exists a slight increase in the resistance baseline and subsequent decrease in the sensor response to CO. These tests were extended to a film stored over a period of 60 days, which also confirms the good sensing stability of both β-Ga_2O_3 nanostructure thin films. From the results, β-Ga_2O_3 with a nanorod shape exhibits excellent sensitivity, stability, reproducibility, response, and recovery time towards CO, when compared to β-Ga_2O_3 with a rectangular shape at 100 °C. This can be attributed to the small particle size, unique shape, interaction between the film and analyte gas behavior.

In general, the gas sensing behaviour of a semiconductor metal oxide depends on the basis of modification of the electrical properties of an active element, which is brought about by the adsorption of an analyte on the surface of the sensor.[40] In the β-Ga_2O_3, a well-known n-type gas sensing material, electrons are the majority carriers and its gas sensing mechanism belongs to the surface-controlled type, the change of resistance is due to the species and the amount of chemisorbed oxygen and gas on the surface (Fig. 10). The stable oxygen ions were O_2^- below 100 °C, O^- between 100 and 300 °C, and O^{2-} above 300 °C,[40] therefore the oxygen ions are adsorbed on the β-Ga_2O_3 surface in the form of O_2^- mainly at the operating temperature of 100 °C in the present work.

Meanwhile, the CO gas sensing properties can be explained by the gas sensing mechanism of β-Ga_2O_3 samples with the change in resistance of the sensor upon exposure to different gas concentrations. When operated at a moderate temperature, the oxygen molecules in air can capture electrons from the β-Ga_2O_3 conduction band and form chemisorbed oxygen species O_2^-, O^-, and O^{2-} (O_2^- is believed to be dominant at 100 °C) on the surface of the sensing layer.[41] When the β-Ga_2O_3 nanostructure is exposed to reduction gas, CO molecules react with the surface of the film releasing the trapped electrons back to the conduction band, and then the resistance of the sensor decreases. The relevant reaction on the surface area could be as follows

$$O_2\,(gas) \Leftrightarrow O_2\,(ads) + e^- \Leftrightarrow O_2^-\,(ads) + e^- \Leftrightarrow 2O^-\,(ads) + e^- \Leftrightarrow O^{2-}\,(ads) + e$$

Now, reduction gas CO flows to the surface of β-Ga_2O_3 samples, the CO molecules adsorb on the β-Ga_2O_3 surface acting as acceptors. These surface accepted lone-pair electrons cause band bending, which decrease the resistance of β-Ga_2O_3 samples as shown in Fig. 7b. The following reaction takes place on the surface of the β-Ga_2O_3 sensing film

$$\beta\text{-}Ga_2O_3 + CO\,(gas) \Leftrightarrow \beta\text{-}Ga_2O_3 - CO\,(ads) \Leftrightarrow \beta\text{-}Ga_2O_3{}^+ - CO^-\,(ads) \Leftrightarrow \beta\text{-}Ga_2O_3 - CO\,(ads) + e^-$$

In addition, enhanced gas sensing performance of β-Ga_2O_3 nanorods compared to that of the rectangular shape can be ascribed to the following reasons. The as-prepared β-Ga_2O_3

nanorods have a small particle size of ~60 nm, which can strongly improve gas sensing performances.[42] That is because a small particle size is directly propositional to a larger surface area and thus provides more surfaces to interact with the target gas. Meanwhile, β-Ga_2O_3 nanostructure thin film samples have more adsorbed oxygen or oxygen in the hydroxyl group as confirmed by the compositional analysis.

4. Conclusion

In summary, a nanostructure β-Ga_2O_3 thin film based CO gas sensor has been successfully synthesized on Si substrates with an inter digital Pd comb-like electrode using a horizontal tubular furnace without using any metal catalyst or additives with optimized parameters. Phase purity, crystallinity, surface morphology, and surface roughness measurements of the prepared samples confirmed the rectangular and rod shape structure with an average size of ~90 nm and 60 nm. The elemental composition analysis indicated that a huge amount of oxygen vacancies appearing on the surface is directly related to the sensor response. Nanostructure β-Ga_2O_3 rod shaped thin films exhibited good sensitivity, high selectivity, excellent stability, repeatability, and response–recovery time to low concentration (1 ppm) of CO at 100 °C when compared to the nanostructure β-Ga_2O_3 rectangular shaped thin films. The above results indicate that the shape and size of the primary nanoparticles, the amount of adsorbed oxygen species and the morphology of the final products would have important influence on their sensitivity. In addition, the results suggest that the prepared nanostructured β-Ga_2O_3 thin films with excellent surface active sites are promising candidates as excellent performance toxic gas sensors.

Acknowledgements

K. G. gratefully acknowledges DRDO-BU CLS, India for the award of Junior Research Fellow and S. T. gratefully acknowledges the Brazilian research funding agency FAPESP (Process 2013/19049-0).

References

1 X. D. Wang, C. J. Summers and Z. L. Wang, *Nano Lett.*, 2004, **4**, 423–426.
2 S. Devan, W. D. Ho, J. H. Lin, S. Y. Wu, Y. R. Ma, P. C. Lee and Y. Liou, *Cryst. Growth Des.*, 2008, **8**, 4465–4468.
3 V. N. T. Satyanarayana, A. S. Kuchibhatla, D. B. Karakoti and S. Seal, *Prog. Mater. Sci.*, 2007, **52**, 699–913.
4 C. Lu, L. Qi, J. Yang, L. Tang, D. Zhang and J. Ma, *Chem. Commun.*, 2006, **33**, 3551–3553.
5 R. Zou, G. He, K. Xu, Q. Liu, Z. Zhang and J. Hu, *J. Mater. Chem. A*, 2013, **1**, 8445–8452.
6 G. Jimenez-Cadena, J. Riu and F. X. Rius, *Analyst*, 2007, **132**, 1083–1099.
7 K. Girija, S. Thirumalairajan, G. S. Avadhani, D. Mangalaraj, N. Ponpandian and C. Viswanathan, *Mater. Res. Bull.*, 2013, **48**, 2296–2303.
8 S. Thirumalairajan, V. R. Mastelaro and C. A. Escanhoela Jr, *ACS Appl. Mater. Interfaces*, 2014, **6**, 21739–21749.
9 K. Girija, S. Thirumalairajan and D. Mangalaraj, *Chem. Eng. J.*, 2014, **236**, 181–190.
10 Y. Zhang, J. Xu, Q. Xiang, H. Li, Q. Pan and P. Xu, *J. Phys. Chem. C*, 2009, **113**, 3430–3435.
11 X. Li, T. Lou, X. Sun and Y. Li, *Inorg. Chem.*, 2004, **43**, 5442–5449.
12 N. Ma, K. Suematsu, M. Yuasa, T. Kida and K. Shimanoe, *ACS Appl. Mater. Interfaces*, 2015, **7**, 5863–5869.
13 X. Sun, H. Hao, H. Ji, X. Li, S. Cai and C. Zheng, *ACS Appl. Mater. Interfaces*, 2014, **6**, 401–409.
14 B. Wang, L. F. Zhu, Y. H. Yang, N. S. Xu and G. W. Yang, *J. Phys. Chem. C*, 2008, **112**, 6643–6647.
15 L. Mazeina, N. Yoosuf, I. Serguei, F. Maximenko, R. Keith, E. Mark and M. Sharka, *Cryst. Growth Des.*, 2009, **9**, 4471–4479.
16 K. Liu, M. Sakurai and M. Aono, *J. Mater. Chem.*, 2012, **22**, 12882–12887.
17 J. S. Kim, H. E. Kim and H. L. Park, *Solid State Commun.*, 2004, **132**, 459–463.
18 N. Ueda, H. Hosono, R. Waseda and H. Kawazoe, *Appl. Phys. Lett.*, 1997, **70**, 3561–3563.
19 K. Girija, S. Thirumalairajan, A. K. Patra, D. Mangalaraj, N. Ponpandian and C. Viswanathan, *Curr. Appl. Phys.*, 2013, **13**, 652–658.
20 Y. Zhao, R. L. Frost and W. N. Martens, *J. Phys. Chem. C*, 2007, **111**, 16290–16299.
21 Y. Zhao, R. L. Frost, J. Yang and W. N. Martens, *J. Phys. Chem. C*, 2008, **112**, 3568.
22 J. Zhang, Z. Liu, C. Lin and J. Lin, *J. Cryst. Growth*, 2005, **280**, 99–106.
23 C. Baban, Y. Toyoda and M. Ogita, *J. Optoelectron. Adv. Mater.*, 2005, **7**, 891–896.
24 S. Thirumalairajan and V. R. Mastelaro, *Sens. Actuators, B*, 2016, **223**, 138–148.
25 Y. Kokubun, K. Miura, F. Endo and S. Nakagomi, *Appl. Phys. Lett.*, 2007, **90**, 031912.
26 S. H. Park, S. H. Kim, S. Y. Park and C. Lee, *RSC Adv.*, 2014, **4**, 63402–63407.
27 Z. Liu, T. Yamazaki, Y. Shen, T. Kikuta, N. Nakatani and Y. Li, *Sens. Actuators, B*, 2008, **129**, 666–670.
28 A. C. Tas, P. J. Majewski and F. Aldinger, *J. Am. Ceram. Soc.*, 2002, **85**, 1421–1429.
29 S. Thirumalairajan, K. Girija, V. R. Mastelaro and N. Ponpandian, *New J. Chem.*, 2014, **38**, 5480–5490.
30 R. Rao, A. M. Rao, B. Xu, J. Dong, S. Sharma and M. K. Sunkara, *J. Appl. Phys.*, 2005, **98**, 094312.
31 H. D. Xiao, H. L. Ma, C. S. Xue, H. Z. Zhuang, F. J. Zong and X. J. Zhang, *Mater. Chem. Phys.*, 2007, **101**, 99–102.
32 H. W. Kim, *Appl. Phys. A*, 2007, **86**, 315–319.
33 Q. Xu and S. Zhang, *Superlattices Microstruct.*, 2008, **44**, 715–720.
34 S. Xiong, B. Xi and Y. Qian, *J. Phys. Chem. C*, 2010, **114**, 14029–14035.
35 C. Jin, J. Lee, K. Baek and C. Lee, *Cryst. Res. Technol.*, 2010, **45**, 1069–1074.

36 S. Katoch, G. Choi and S. Kim, *J. Mater. Chem. A*, 2013, **1**, 13588–13596.
37 L. Wang, Y. Kang, Y. Wang, B. Zhu, S. Zhang and W. Huang, *Mater. Sci. Eng., C*, 2012, **32**, 2079.
38 Y. Liu, G. Zhu, J. Chen, H. Xu, X. Shen and A. Yuan, *Appl. Surf. Sci.*, 2012, **265**, 379–384.
39 W. Wang, Z. Li, W. Zheng, H. Huang, C. Wang and J. Sun, *Sens. Actuators, B*, 2010, **143**, 754–759.
40 H. Altunas, I. Donmez, C. Ozgit and N. Biyikli, *J. Alloys Compd.*, 2014, **593**, 190–195.
41 S. Thirumalairajan, K. Girija, V. R. Masterlo and N. Ponpandian, *ACS Appl. Mater. Interfaces*, 2014, **6**, 13917–13927.